



Uncertainty Quantification of Microstructural Properties due to Experimental Variations

Pinar Acar* and Veera Sundararaghavan†
University of Michigan, Ann Arbor, Michigan 48109

DOI: 10.2514/1.J055689

Electron backscatter diffraction scans are an important experimental input for microstructure generation and homogenization. Multiple electron backscatter diffraction scans can be used to sample the uncertainty in orientation distribution function: both point to point within a specimen as well as across multiple specimens that originate from the same manufacturing process. However, microstructure analysis methods typically employ only the mean values of the orientation distribution function to predict properties, and the stochastic information is lost. In this work, analytical methods are developed to account for the uncertainty in the electron backscatter diffraction data during property analysis. To this end, a linear smoothing scheme is developed in the Rodrigues fundamental region to compute the orientation distribution function from the electron backscatter diffraction data. The joint multivariate probability distributions of the orientation distribution function are then modeled using a Gaussian assumption. The uncertainty in engineering properties that are obtained by homogenization are also computed. It is shown that the uncertainty in nonlinear properties can be analytically obtained using direct transformation of random variables in the homogenization approach.

I. Introduction

ONE of the pillars of integrated computational materials engineering (ICME) (Allison et al. [1]) is uncertainty quantification (UQ), and it involves development of mathematical tools to quantify the effect of the stochasticity of a microstructure on the predicted engineering properties. Microstructural uncertainties arise from imperfections in the manufacturing processes, such as variations in the stress or temperature gradients during forming processes used to make aircraft components such as turbine disks. These imperfections lead to stochasticity, both point to point within a specimen as well as across multiple specimens that originate from the same manufacturing process. In the UQ parlance, these uncertainties are classified as “aleatoric.” Electron backscatter diffraction (EBSD) is an important experimental method to quantify such microstructural variations. We employ multiple EBSD scans on alloy specimens made from the same manufacturing process to sample the various microstructures. The goal of this paper is to model the propagation of these uncertainties on engineering properties using an analytical approach.

The current state of the art to model the uncertainties in materials involves the use of expensive numerical simulations such as the Monte Carlo simulation (MCS), collocation, and spectral decomposition methods. Creuziger et al. [2] examined the uncertainties in the ODF values of a microstructure due to the variations in the pole figure values by using a MCS. Juan et al. [3] used the MCS to study the effects of a sampling strategy on the determination of various characteristic microstructure parameters, such as grain size distribution and grain topology distribution. Hiriyur et al. [4] studied an extended finite element method coupled with an MCS approach to quantify the uncertainties in the homogenized effective elastic properties of multiphase materials. Kouchmeshky and Zabaraz [5] presented the propagation of initial texture and deformation process uncertainties on the final product properties using a stochastic collocation approach.

Madrid et al. [6] examined the variability and sensitivity of an in-plane Young’s modulus of thin nickel polycrystalline films due to uncertainties in the microstructure geometry and crystallographic texture, as well as numerical values of single crystal elastic constants, by using a numerical spectral technique. Niezgoda et al. [7] computed the variances of the microstructure properties by defining a stochastic process to represent the microstructure. Some authors have also focused on the computational techniques to study the uncertainties on microstructural homogenization approaches. Huysse and Maes [8] studied the effect of microstructural uncertainties on homogenized parameters by using random windows from the real microstructure, and they performed a MCS to identify the stochasticity in elastic parameters such as Young’s modulus and Poisson’s ratio. Sakata et al. [9] also showed the variations in Young’s modulus and Poisson’s ratio due to microscopic uncertainties. They validated the results of their perturbation-based homogenization method with the MCS. In another paper, Sakata et al. [10] implemented a kriging approach to calculate the probability density functions of the material properties, and they used a MCS to study the uncertainties in the geometry and material properties of a microstructure through the same perturbation-based homogenization method. A computational stochastic modeling approach for random microstructure geometry was presented by Clement et al. [11,12]. The authors presented a high-dimensional problem due to the high number of stochastic variables to represent the microstructure geometry. This high-dimensionality was reduced with the implementation of a polynomial chaos expansion.

These computational methods presented in the literature involve using a numerical algorithm for uncertainty quantification and propagation. They represent the joint probability distributions of uncertain variables either using interpolation functions or sampling for random points. These techniques are not as computationally efficient because the problem complexity or the number of variables increases because the number of interpolation terms or sampling points will also increase. This is especially true for orientation distribution functions (ODFs) that are discretized using finite element nodes or spectral basis and contain a large number of free parameters for which the joint distribution needs to be sampled. Another drawback is the difficulty of satisfying design constraints (such as volume fraction normalization) when using numerical approaches. All these disadvantages imply the necessity of developing analytical solutions as a first step in UQ. Recently, we employed the use of Gaussian characteristic functions to stochastically model pole figure inversion [13]. The approach is fully analytical and significantly faster than numerical approaches. However, pole figure inversion is nonunique and leads to “epistemic” uncertainty due to lack of an exact solution. In this paper, we focus on EBSD to ODF conversion,

Presented as Paper 2017-0815 at the 19th AIAA Non-Deterministic Approaches Conference, Grapevine, TX, 9–13 January 2017; received 7 November 2016; revision received 3 February 2017; accepted for publication 6 February 2017; published online 30 June 2017. Copyright © 2017 by Pinar Acar. Published by the American Institute of Aeronautics and Astronautics, Inc., with permission. All requests for copying and permission to reprint should be submitted to CCC at www.copyright.com; employ the ISSN 0001-1452 (print) or 1533-385X (online) to initiate your request. See also AIAA Rights and Permissions www.aiaa.org/randp.

*Graduate Research Assistant, Department of Aerospace Engineering, Student Member AIAA.

†Associate Professor, Department of Aerospace Engineering, Member AIAA.

which is a one-to-one map that is only constrained by the level of discretization of the ODF, and thus aleatoric uncertainties can be better quantified. We employ the Gaussian model and analytically propagate the uncertainties in the ODF to linear and nonlinear properties derived from the ODF. The organization of this paper is as follows. Section II discusses the problem statement. In Sec. III, the mathematical methods are described. Results and conclusions are addressed in Secs. IV and V, respectively.

II. Mathematical Background

The complete orientation space of a polycrystal can be reduced to a smaller subset, called the fundamental region (Fig. 1), as a consequence of crystal symmetries. Within the fundamental region, each crystal orientation is represented uniquely by a coordinate r , which is the parametrization for the rotation (e.g., Euler angles, Rodrigues vector, etc.). The ODF, represented by $\mathcal{A}(r)$, describes the volume density of crystals of orientation r . The fundamental region is discretized into N independent nodes with N_{elem} finite elements (and N_{int} integration points per element), as shown in Fig. 1.

The ODF is normalized to unity over the fundamental region as follows:

$$\int_{\mathcal{R}} \mathcal{A} \, dv = \sum_{n=1}^{N_{\text{elem}}} \sum_{m=1}^{N_{\text{int}}} A(r_m) w_m |J_n| \frac{1}{(1 + r_m \cdot r_m)^2} = 1 \quad (1)$$

where $A(r_m)$ is the value of the ODF at the m th integration point with global coordinate r_m of the n th element, $|J_n|$ is the Jacobian determinant of the n th element, and w_m is the integration weight associated with the m th integration point. This is equivalent to the linear constraint $q^{\text{int}} A^{\text{int}} = 1$, where

$$q_i^{\text{int}} = w_i |J_i| \frac{1}{(1 + r_i \cdot r_i)^2}$$

and $A_i^{\text{int}} = A(r_i)$, where $i = 1, \dots, N_{\text{int}} \times N_{\text{elem}}$.

If the orientation-dependent property for single crystals $\chi(r)$ is known, any polycrystal property can be expressed as an expected value, or average, over the ODF as follows:

$$\langle \chi \rangle = \int \chi(r) A(r) \, dv \quad (2)$$

This equation can be expressed in a linear form as follows:

$$\langle \chi \rangle = \int_{\mathcal{R}} \chi(r) A(r) \, dv = \sum_{n=1}^{N_{\text{elem}}} \sum_{m=1}^{N_{\text{int}}} \chi(r_m) A(r_m) w_m |J_n| \frac{1}{(1 + r_m \cdot r_m)^2} \quad (3)$$

This is again equivalent to an equation linear in the ODF of $\langle \chi \rangle = p^{\text{int}} A^{\text{int}}$, where

$$p_i^{\text{int}} = \chi(r_i) w_i |J_i| \frac{1}{(1 + r_i \cdot r_i)^2}$$

and $A_i^{\text{int}} = A(r_i)$, $i = 1, \dots, N_{\text{int}} \times N_{\text{elem}}$.

Using reduced integration with one integration point per element at a local coordinate of (0.25, 0.25, 0.25) and an integration weight of $w = 1/6$, the simplified property matrix p^{int} corresponding to polycrystal average properties $\{\langle \chi \rangle\}$ is given as follows:

$$p^{\text{int}} = \begin{bmatrix} \frac{1}{6} \chi_1(r_1) |J_1| \frac{1}{(1+r_1 \cdot r_1)^2} \\ \frac{1}{6} \chi_1(r_2) |J_2| \frac{1}{(1+r_2 \cdot r_2)^2} \\ \dots \\ \frac{1}{6} \chi_1(r_{N_{\text{el}}}) |J_{N_{\text{el}}}| \frac{1}{(1+r_{N_{\text{el}}} \cdot r_{N_{\text{el}}})^2} \end{bmatrix}$$

Crystallographic symmetry is enforced by considering the set of independent nodal points instead of the integration points. Independent nodal points are the reduced set of nodes obtained by accounting for

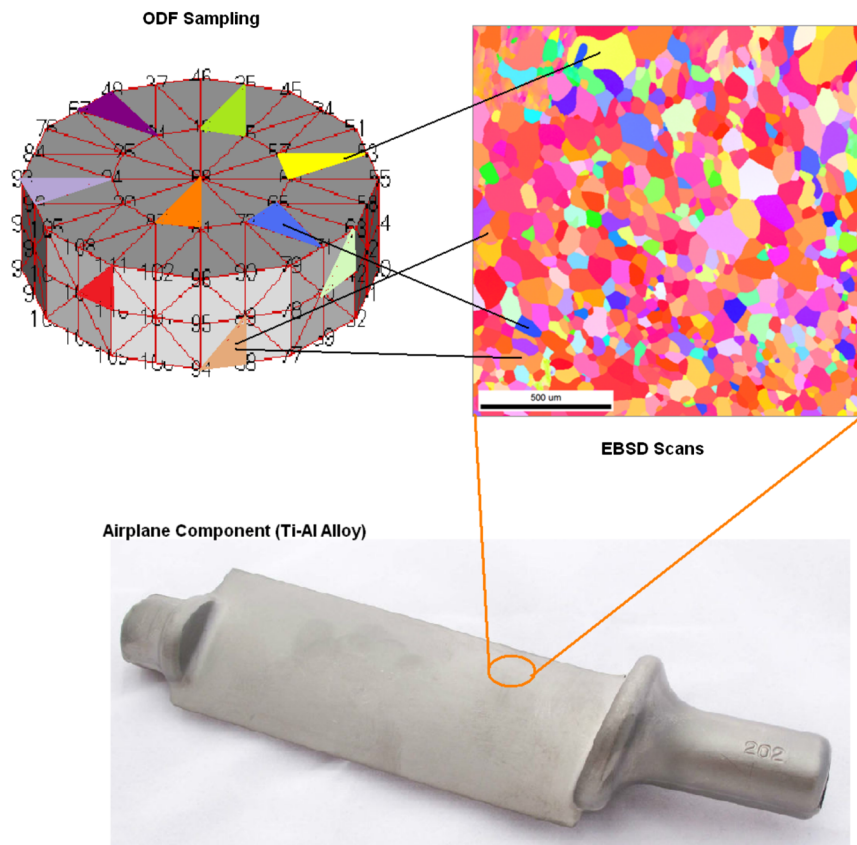


Fig. 1 Representation of the ODF calculation from the orientations obtained with the EBSD data.

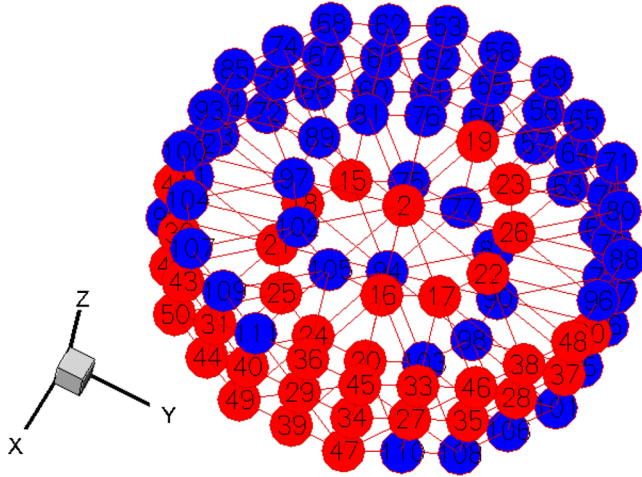


Fig. 2 ODF representation in the Rodrigues fundamental region for hexagonal crystal symmetry, showing the location of the $k = 50$ independent nodes of the ODF in red color.

symmetry conditions at the boundaries of the ODF (see Fig. 2). Let matrix H be such that it converts the independent nodal values to the integration point values $A_e^{\text{int}} = HA^{\text{node}}$. The H matrix can be defined from the equation

$$A_e^{\text{int}} = 0.25 \sum_{i=1}^4 A_e^i$$

where A_e^{int} is the integration point ODF value at element e ; and A_e^i , $i = 1, \dots, 4$ refers to the ODF values at the four nodes of the tetrahedral element e . The p matrix is formed as $p = H^T p^{\text{int}}$ so that any property d can be represented as the scalar product $p^T A^{\text{node}}$.

The orientations from the EBSD data are binned pixel by pixel to the element containing the orientation, and specifically to the integration point in the element. After binning is complete, the ODF value A_i^{int} at the integration point in an element i contains the total number of pixels in the EBSD image that have orientations lying within the element. The data are then normalized by $q^{\text{int}} A_i^{\text{int}}$. Let matrix T convert the integration point values A_i^{int} to the independent nodal values A^{node} , i.e., $A^{\text{node}} = TA^{\text{int}}$. Using one integration point, this matrix is defined as $T_{ij} = \delta_{ij}/f$, where δ_{ij} is one if node i (or its symmetric equivalent) is a vertex of element j and zero otherwise. The factor f is the number of elements with node i (or symmetric equivalent) as one of its vertices. This matrix is always positive; thus, $A^{\text{node}} \geq 0$. The vector containing the values of the ODF at $k - 1$ independent nodal points is hereafter referred to as A .

To account for the normalization constraint, the property vector p is adjusted such that $p_i = p_i - (p_k q_i / q_k)$ for $i = 1, \dots, k - 1$, and the property rewritten as

$$\langle \chi \rangle = \sum_{i=1}^{k-1} p_i A_i + \frac{p_k}{q_k} = p^T A + r$$

Other properties may be derived from $\langle \chi \rangle$. For example, the elastic modulus can be written as $E = (1/\langle S_{11} \rangle)$, where $\langle S_{11} \rangle$ is a component of the compliance matrix S computed from the lower bound relation:

$$\langle S \rangle = \int_R S(r) A(r) dv$$

Given the uncertainty in the EBSD data, the primary goals of this paper are as follows:

1) Develop analytical forms for the probability distribution function of the ODF.

2) Compute the uncertainty in properties derived from the homogenization equation [Eq. (2)] given the uncertainty in the ODF.

The probabilistic methods employed are explained next.

III. Methods

In this work, the experimental EBSD scans for a titanium alloy were considered to determine the ODF values. The variabilities in the ODFs were computed from 150 different samples drawn from the specimen. Some of the example EBSD samples are shown in Fig. 3. The ODFs were calculated from the EBSD data by binning the values at integration points. The ODF values at the independent nodal points were then obtained using the linear relation between nodal point and integration point ODFs. The histograms of the experimental variations were plotted, and we found the variability in the ODFs could be modeled with a bell-shaped distribution: e.g., of the Gaussian type, as shown in Fig. 4, for some of the integration point ODFs. The skewness of the integration point probability distributions are also calculated, and it is shown in Fig. 5 that they vary around zero, which is the skewness value of the Gaussian distribution. As shown in Fig. 5, most of the skewness values are very close to zero, and the maximum absolute difference with the Gaussian skewness value is only around 0.15. This result also proves that the ODFs can be modeled with a Gaussian distribution because it shows that the probability distributions of the integration point ODFs have more of a symmetric characteristic rather than demonstrating a dominant positively or negatively skewed feature. The selection of the Gaussian distribution to model the integration point ODFs is finally checked with probability-probability (P-P) and quantile-quantile (Q-Q) plots [14]. The P-P plot depicts two cumulative distribution functions (CDFs) against each other; it is also being used as another measure to compare the skewness of different distributions. Here, the P-P plot is shown in Fig. 6 to compare the CDFs of the experimental samples and the analytical assumption with Gaussian distribution. The Q-Q plot, on the other hand, is a graphical technique to compare the probability distributions by plotting their quantiles against each other. Figure 6 shows the P-P and Q-Q plots of the experimental samples and the Gaussian assumption for some of the example integration point ODFs (the other ODF distributions also represent very similar features). All the tests illustrated in Figs. 4–6 show that the variations of the integration point ODFs in the experimental samples agree well with a Gaussian distribution assumption.

The Gaussian approximation allows for development of analytical expressions while considering correlations between the various ODF values. The solution includes two basic steps: The first step is to find the statistical features of linear material properties, and the second step is to find the probability distributions of nonlinear material properties using transformation of random variables.

A. Computation of the Property Uncertainty Using Gaussian Distributed Correlated Variables

The Gaussian approach, which can model all k correlated ODF nodal variables, is used to represent the uncertainties in EBSD data.

Assume a d -dimensional multivariate Gaussian distribution: $X \sim N_d(\mu, \Sigma)$. Now, we define a new random variable:

$$Z = AX = \sum_{i=1}^d \sum_{j=1}^d a_{ij} X_j \quad (4)$$

where A is a constant matrix. Here, Z is Gaussian distributed. The mean and covariance of Z are given by the following:

$$\mu_Z = A\mu_X \quad (5)$$

$$\Sigma_Z = A\Sigma_X A^T \quad (6)$$

The Gaussian approach presented here can be modified accordingly to represent the variations in the ODFs and linear material properties. The formulation to compute the mean and variance of the ODFs at $k - 1$ independent nodal points using the ODFs at the integration points is given as follows:

$$\mu_A = T^* \mu_{A^{\text{int}}} \quad (7)$$

$$\Sigma_A = T^* \Sigma_{A^{\text{int}}} T^{*T} \quad (8)$$

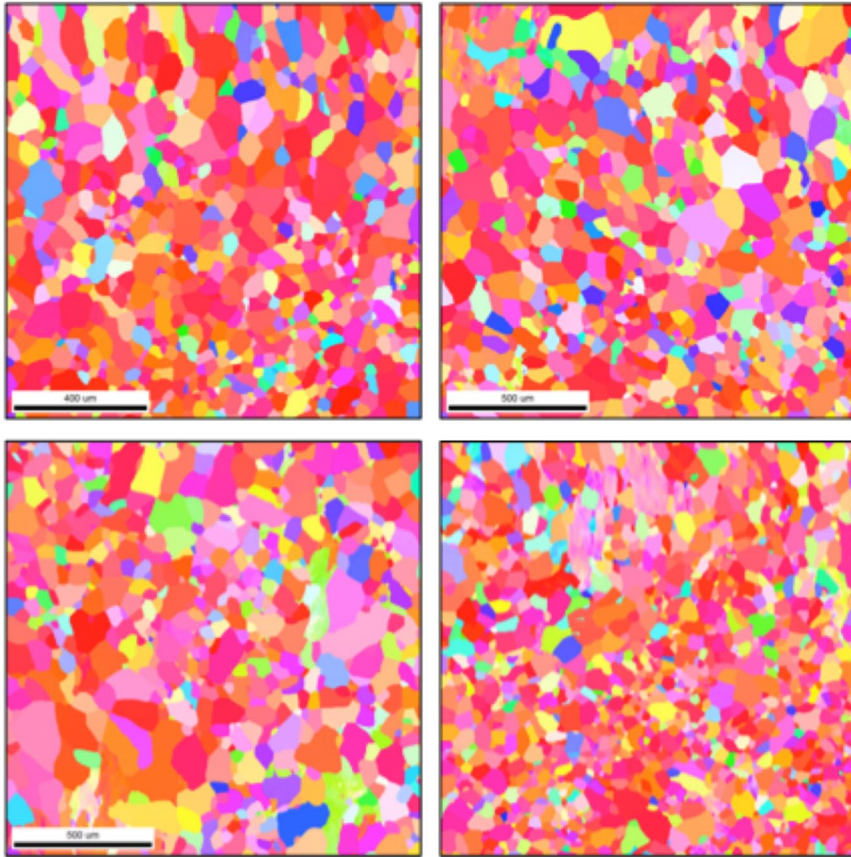


Fig. 3 Some example EBSD samples.

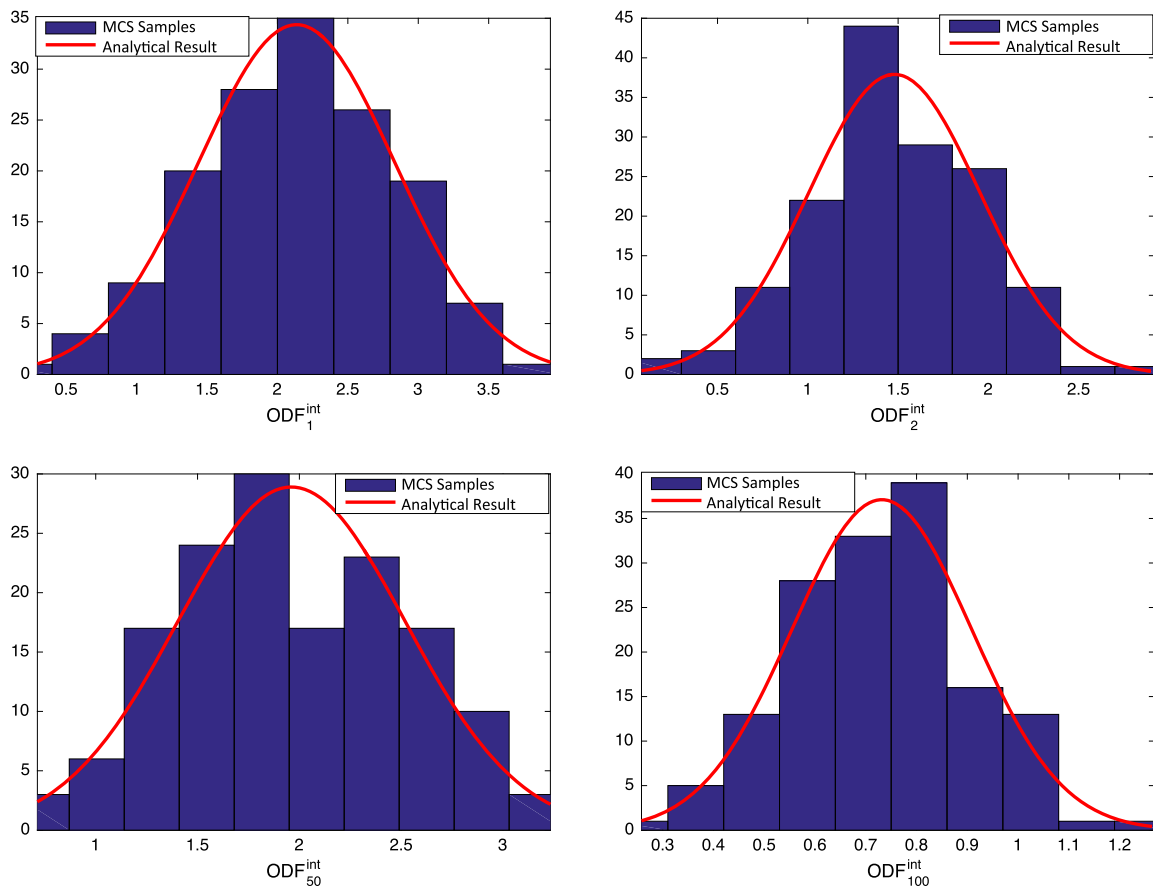


Fig. 4 ODFs at the integration points agreeing with the Gaussian distribution.

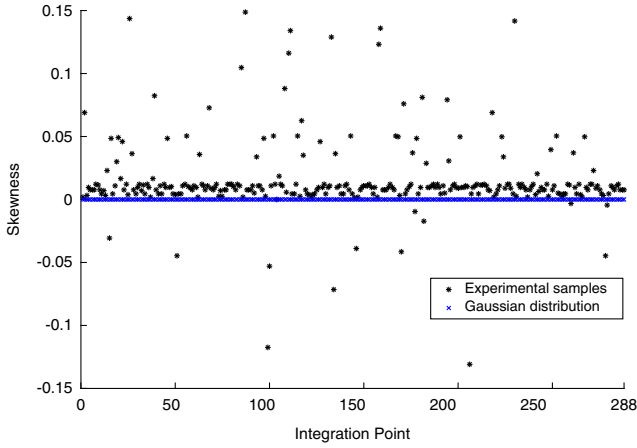


Fig. 5 Skewness of the integration point ODF variations.

where μ_A and Σ_A are the mean and covariance of the ODF at $k - 1$ independent nodal points, T^* is matrix T with the first $k - 1$ rows included. $\mu_{A^{int}}$ and $\Sigma_{A^{int}}$ are the mean and covariance of the ODFs at the integration points. Although not required for further analysis, the mean and variance of the k th independent node may be computed from the mean and covariance of the $k - 1$ nodes using the normalization constraint as shown in the Appendix.

The same approach can be followed to compute the uncertainties in the linear material properties. The linear variables chosen for this study are the compliance parameters S_{11} and S_{66} . The mean and variance equations for S_{11} can be shown as follows using the Gaussian approach. The same computation also applies to the statistical parameters of S_{66} :

$$E[S_{11}] = p^T \mu_A + r \tag{9}$$

$$\sigma^2[S_{11}] = p \Sigma_A p^T \tag{10}$$

where p represents the property matrix for S_{11} .

B. Uncertainties in the Nonlinear Material Properties

When the probability distribution of a property is not linear in the ODF, the probability density function (PDF) can still be computed using the transformation of random variables. Given the input

parameter x and the output parameter y , we assume that the relation between x and y can be identified using $y = h(x)$, and it can be inverted as $x = u(y)$. This method computes a Jacobian value J based on this explicit relation (where $J = du/dy$), and it finds the PDF of the output variable as a product of the input PDF and the Jacobian. Equation (11) shows the computation of the output PDF:

$$f_y(y) = f_x[u(y)] \times |J| \tag{11}$$

where f_x and f_y are the PDFs of input and output variables, respectively. Because the input PDF f_x and inverted function $u(y)$ are already known, the output PDF f_y can be computed using this method. Then, the expected value $E[y]$ and variance σ_y^2 of the output parameter can be calculated using Eqs. (12) and (13), respectively [15]:

$$E[y] = \int_{y_{min}}^{y_{max}} y f_y(y) dy \tag{12}$$

$$\sigma_y^2 = E[(y - E[y])^2] \tag{13}$$

where y_{min} and y_{max} are the minimum and maximum values of that the output variable y can take. These values can be computed analytically using the explicit relation $y = h(x)$. The approach is first demonstrated in the next section for computing the PDF of the homogenized elastic modulus $E_1 = 1/S_{11}$ and shear modulus $G_{12} = 1/S_{66}$. The same method is then used to compute the PDFs of the first torsion and bending natural frequencies of a cantilever beam. The cantilever beam problem is the same as the problem in an earlier work of the authors' [16]. However, this time, the beam material is Titanium-7 weight% Aluminum alloy (Ti-7Al). The corresponding equations for the torsion and bending natural frequencies are as follows:

$$\omega_{1t} = \frac{\pi}{2L} \sqrt{\frac{G_{12}J}{\rho I_p}}$$

and

$$\omega_{1b} = (\alpha L)^2 \sqrt{\frac{E_1 I_1}{m L^4}}$$

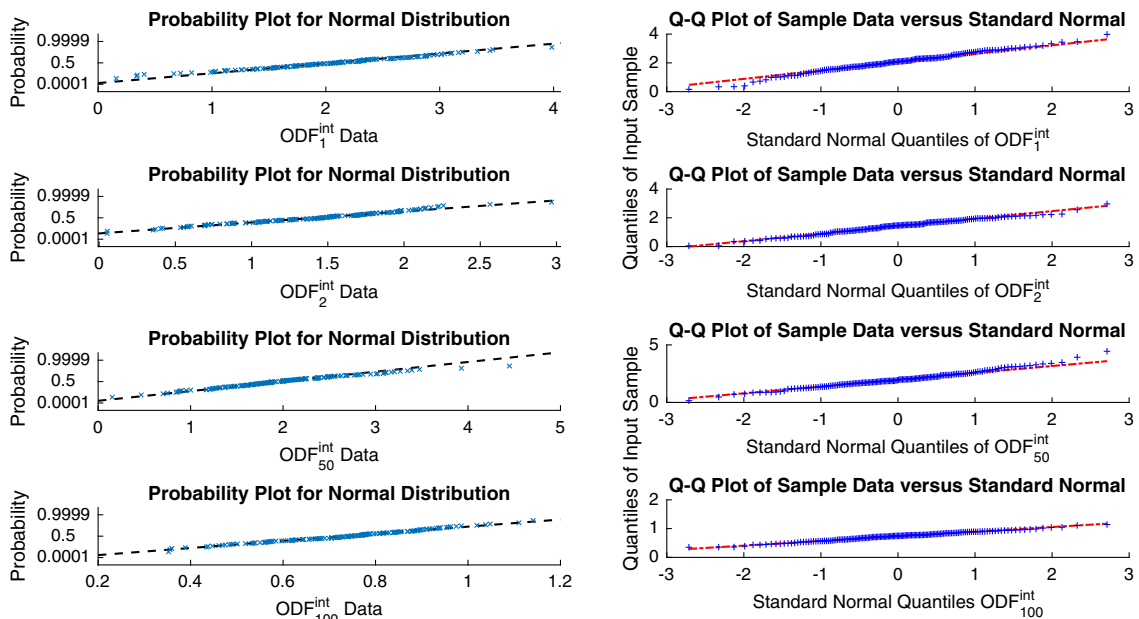


Fig. 6 P-P and Q-Q plots of the experimental samples and Gaussian assumption.

respectively. In these equations, J is the torsion constant, ρ is density, I_p is the polar inertia moment, m is the unit mass, L is the length of the beam, and I_1 is the moment of inertia along axis 1 [16]. To compute the probability distributions of ω_{1t} and ω_{1b} , the geometrical beam properties given in the previous work [16] are considered.

IV. Results and Discussion

This section discusses quantification of uncertainties introduced to the ODFs due to the variations in the experimental samples. Three different samples of Ti-7Al alloy were taken from different regions of a beta-forged ingot. The original samples were taken from different regions of the ingot, creating variability in the resulting microstructure due to the inhomogeneity of the forging process. These samples were subject to the same thermomechanical process. All three samples were compressed to a 20% height reduction at room temperature, and they were annealed for 72 h at 1073 K. The compression direction was also the longitudinal direction of the forging. Scans were taken from different regions of the processed samples. A total of 150 small scans were generated from these scans to represent the statistical features of the ODFs sufficiently. Representative samples indicated a weakly basal texture. The Hexagonal close packed fundamental region discretized with 50 independent nodes was used to model the ODF. Using the experimental EBSD scans, the ODFs were obtained by binning to the elements. Using multiple scan data, we obtained a histogram of ODF values at the integration points. The experimental samples were shown to be modeled with a Gaussian distribution assumption because the histograms, skewness, and P-P and Q-Q plots agreed with the Gaussian features. The mean and covariance of the ODFs at the 49 independent nodes were then computed by applying the

Gaussian approach. We computed the probability distribution of the last ODF (ODF₅₀) by using the volume fraction normalization constraint. The histograms for some of the ODFs, including the last ODF (ODF₅₀) are shown in Fig. 7. ODF₅₀ in particular had a lower standard deviation due to the normalization constraint. The statistical properties of the ODF distributions (mean values, standard deviations, and coefficient of variations of the ODFs) are plotted on the mesh in Fig. 8. We found that some of the ODF values with high mean values also had higher standard deviations, but there were still some other ODFs with high standard deviations and relatively lower mean values because of the larger experimental variations for those nodes. Thus, the coefficient of variation (ratio of standard deviation to mean) of the ODFs was not entirely uniform because the higher-density areas indicated the ODFs with relatively higher standard deviations as compared to their mean values.

The uncertainties in the ODFs and material properties are quantified using the MCS and a Gaussian distribution model to compare the results of the analytical model. In the MCS approach, we used the aforementioned 150 experimental samples and directly computed the ODFs from each set. Then, 150 sets of material properties (S_{11} , E_1 , etc.) were computed from these ODFs using the homogenization relation [Eq. (2)]. Histograms of these ODFs and properties were directly compared to the Gaussian analytical solution. The analytical solution was much faster; the solution times were around 7 s for analytical models and 20 min for a MCS on the same computational platform. However, the MCS provided exact solutions because no Gaussian PDF approximation was made. The Gaussian analytical solution assumed that all the ODF values were correlated. Thus, we used a full covariance matrix to model the ODFs with the Gaussian approach. The MCS results for the probability

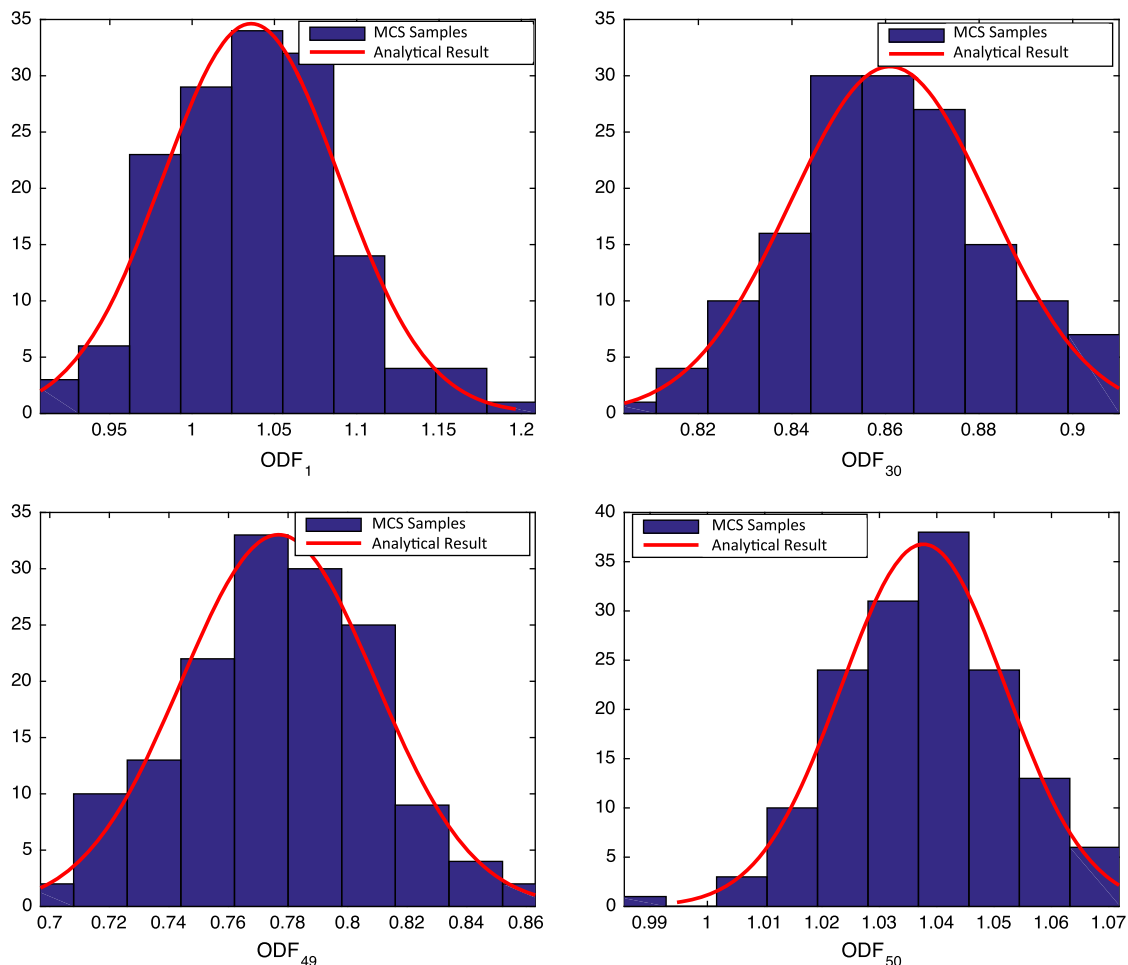


Fig. 7 Probability histograms of the ODFs.

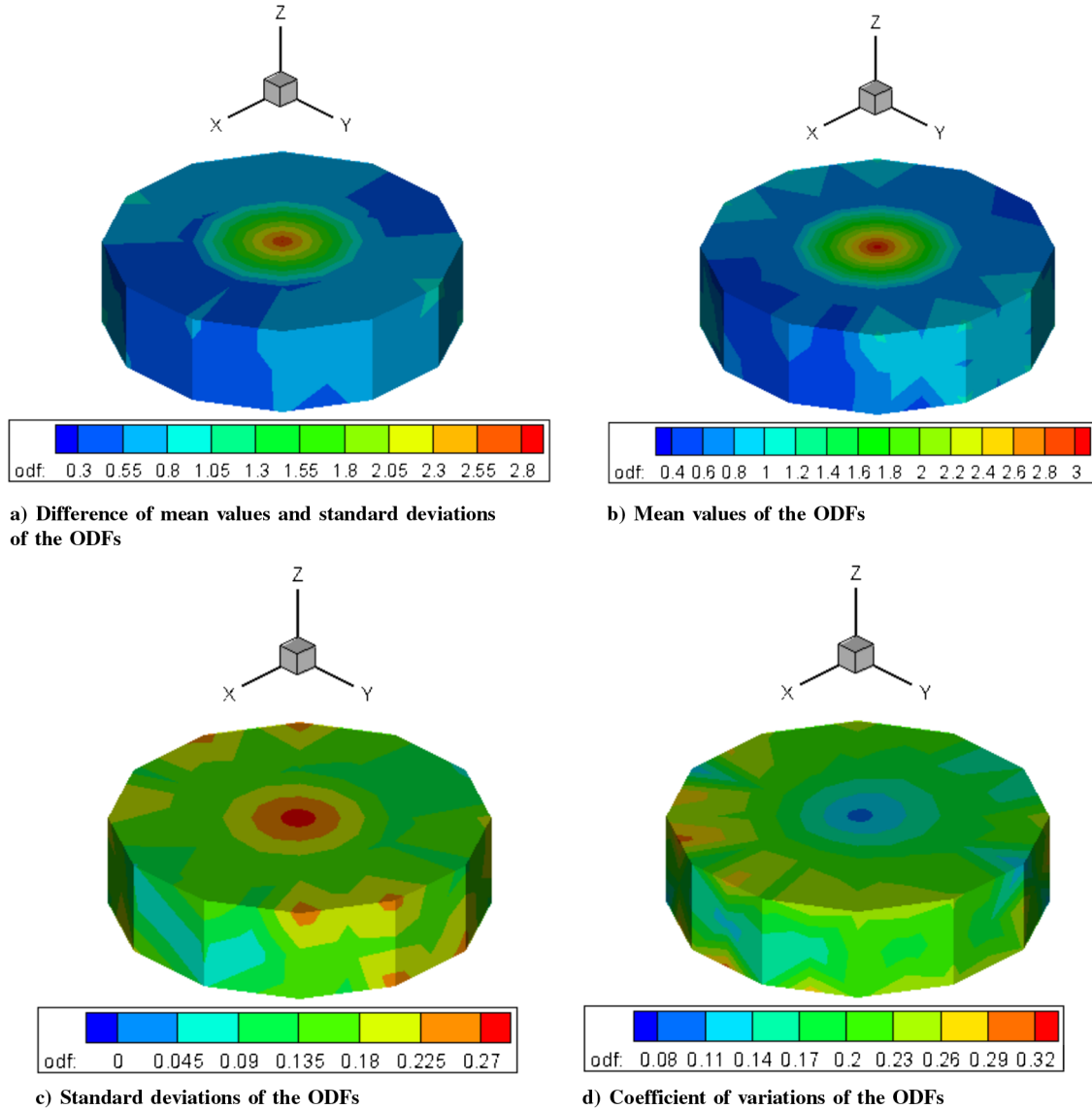


Fig. 8 Statistical features of the ODF probability distributions.

distributions of S_{11} , S_{66} , E_1 , G_{12} , ω_{1r} , and ω_{1b} are shown together with the analytical model results in Fig. 9.

Knowing the uncertainty in the ODF, the uncertainties in the homogenized properties were quantified using the analysis in Sec. III with Gaussian distribution. The compliance elements, S_{11} and S_{66} , were computed using the lower-bound approximation. The elastic constants of the single crystals were considered for 750°C [17], and the values were taken as $C_{11} = 125.3$ GPa, $C_{12} = 99.4$ GPa, $C_{13} = 68.8$ GPa, $C_{33} = 154.5$ GPa, and $C_{55} = 31.6$ GPa. The linear features of the Gaussian distribution were implemented to compute the expected value and covariance. The probability distributions of S_{11} and S_{66} are shown in Fig. 9. The full covariance matrix was again computed to identify the distributions of S_{11} and S_{66} .

The next step considers the PDFs of the Young's Modulus along a sample x direction E_1 and shear modulus G_{12} . Even though the probability distributions of S_{11} and S_{66} are modeled with Gaussian distributions, the probability distributions of E_1 and G_{12} are not Gaussian due to their inverse relations ($E_1 = 1/S_{11}$ and $G_{12} = 1/S_{66}$). The PDFs of E_1 and G_{12} are determined using the transformation of random variables [Eq. (11)] in Sec. III.B. To compute these PDFs, the transformation function can be identified as $u(y) = 1/y$ according to the relations between E_1 and S_{11} , and G_{12}

and S_{66} . Then, the expected values and the variances are calculated using Eqs. (12) and (13). Similarly, the PDF of the first torsion and bending natural frequencies are computed using a transformation function of $u(y) = a\sqrt{y}$, where a is a constant due to the relations between G_{12} and ω_{1r} , and E_1 and ω_{1b} . The probability distributions of E_1 , G_{12} , ω_{1r} , and ω_{1b} are also shown in Fig. 9.

The overall analysis is fully analytical when using the Gaussian distribution. However, a drawback of the Gaussian distribution is that it allows for negative variables. All the variables considered here (i.e., ODFs, and linear and nonlinear properties) are all positive. There are several available distribution models satisfying this nonnegativity condition, such as log-normal, exponential, Weibull, and Rayleigh distributions. However, the exact analytical treatment of the linear system of equations of correlated random variables is not available for positive PDFs in the literature. Thus, going beyond Gaussian distributions, one needs to also pursue numerical methods such as the MCS and collocation techniques for exact UQ. From our MCS analysis, we see that the mean values of the probability distributions computed with a MCS are in very good agreement with the distributions of the analytical model for the ODFs and material properties in Fig. 9. The variances of the material properties modeled with the analytical model are also compatible with the MCS data. It is also much faster, which is important when stochastic ODFs are

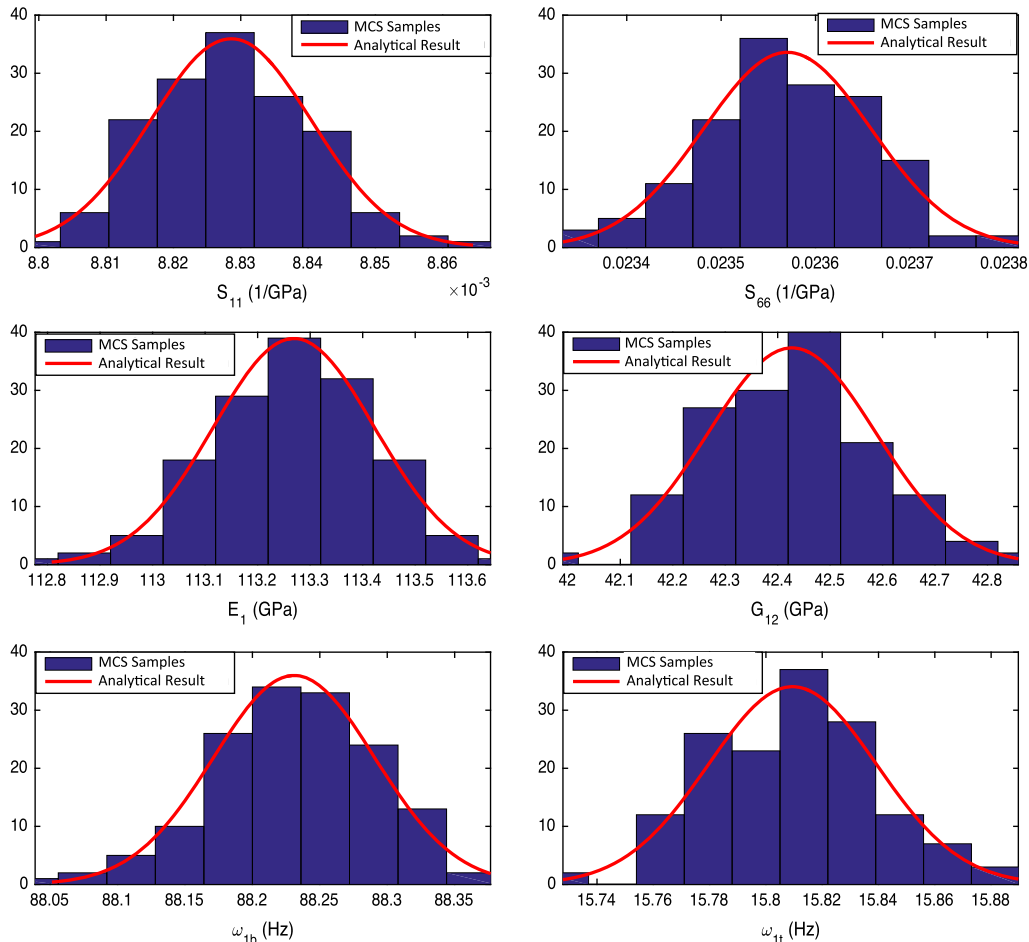


Fig. 9 Probability histograms of S_{11} , S_{66} , E_1 , G_{12} , ω_{1t} , and ω_{1b} .

employed in multiscale formulations [18] of thermomechanical processes.

V. Conclusions

Analytical techniques for quantification of experimental uncertainties on material properties of microstructures as obtained from volume-averaged homogenization relationships were addressed. The uncertainties in experimental Electron backscatter diffraction scans were identified using titanium alloy specimens that were obtained identically through the same process. The uncertainties in the ODF values were quantified using 150 equally sized diffraction samples, and they were fitted to a Gaussian distribution. The probability distribution of the last ODF parameter was computed using a volume fraction normalization constraint. The probability distributions of the linear properties, including the last ODF and the compliance parameters, were calculated using the linear homogenization equations. The mathematical model for the probability distributions of nonlinear properties was identified using the transformation of random variables. Using this approach, the uncertainty bounds were calculated for the Young's modulus, the shear modulus, the first torsion, and the bending natural frequencies of the titanium alloy specimen, which will be useful for an engineering analysis. These derivations were important for development of an integrated computational materials engineering toolbox for computing the uncertainty in multiscale homogenization models due to input uncertainties. An analytical approach has the drawback of having an infinite support space compared to the finite support of the discretized ODFs and properties. However, these methods provided a considerable reduction in computational times as compared to available numerical techniques. Thus, it is recommended that the Gaussian approach

presented here be used as a first step to verify more advanced uncertainty quantification models.

Appendix: Derivation of Statistical Features for Correlated Variables

To satisfy the normalization constraint, the equations to compute the statistical properties of the k th independent node are modified. The mean and variance of the k th ODF value can be obtained as

$$E[A_k] = c^T \mu_A + \frac{1}{q_k}$$

and

$$\sigma^2[A_k] = c^T \Sigma_A c$$

where $c_i = -(q_i/q_k)$, and μ_A and Σ_A are the mean and covariance of $k-1$ independent nodes, as computed in Eqs. (7) and (8). After the modification for the k th variable, the full ODF covariance matrix can be written as follows:

$$\Sigma_A^* = \begin{bmatrix} \Sigma_A & S \\ S^T & \sigma_k^2 \end{bmatrix} \quad (\text{A1})$$

where S is a column vector for which the values are given by the following:

$$S_i = -\frac{1}{q_k} \sum_{j=1}^{k-1} q_j (\Sigma_A)_{ij} \quad (\text{A2})$$

Acknowledgments

The work presented here was funded by the Office of Naval Research grant N00014-12-1-0013. The computations have been carried out as part of research supported by the U.S. Department of Energy, Office of Basic Energy Sciences, Division of Materials Sciences and Engineering under award no. DE-SC0008637, which funds the Predictive Integrated Structural Materials Science Center at the University of Michigan. The authors would like to thank Anna Trump (Graduate Research Assistant in John Allison's research group in the Materials Science and Engineering Department of the University of Michigan) for providing the experimental data.

References

- [1] Allison, J., Backman, D., and Christodoulou, L., "Integrated Computational Materials Engineering: A New Paradigm for the Global Materials Profession," *Journal of the Minerals, Metals and Materials Society*, Vol. 58, No. 11, 2006, pp. 25–27.
doi:10.1007/s11837-006-0223-5
- [2] Creuziger, A., Syed, K., and Gnaupel-Herold, T., "Measurement of Uncertainty in Orientation Distribution Function Calculations," *Scripta Materialia*, Vols. 72–73, Feb. 2014, pp. 55–58.
doi:10.1016/j.scriptamat.2013.10.017
- [3] Juan, L., Liu, G., Wang, H., and Ullah, A., "On the Sampling of Three-Dimensional Polycrystalline Microstructures for Distribution Determination," *Journal of Microscopy*, Vol. 44, No. 2, 2011, pp. 214–222.
- [4] Hiriyur, B., Waisman, H., and Deodatis, G., "Uncertainty Quantification in Homogenization of Heterogeneous Microstructures Modeled by XFEM," *International Journal for Numerical Methods in Engineering*, Vol. 88, No. 3, 2011, pp. 257–278.
doi:10.1002/nme.3174
- [5] Kouchmeshky, B., and Zabarar, N., "The Effect of Multiple Sources of Uncertainty on the Convex Hull of Material Properties of Polycrystals," *Computational Materials Science*, Vol. 47, No. 2, 2009, pp. 342–352.
doi:10.1016/j.commatsci.2009.08.010
- [6] Madrid, P. J., Sulsky, D., and Lebensohn, R. A., "Uncertainty Quantification in Prediction of the In-Plane Young's Modulus of Thin Films with Fiber Texture," *Journal of Microelectromechanical Systems*, Vol. 23, No. 2, 2014, pp. 380–390.
doi:10.1109/JMEMS.2013.2279500
- [7] Niezgodna, S. R., Yabansu, Y., and Kalidindi, S. R., "Understanding and Visualizing Microstructure and Microstructure Variance as a Stochastic Process," *Acta Materialia*, Vol. 59, No. 16, 2011, pp. 6387–6400.
doi:10.1016/j.actamat.2011.06.051
- [8] Huyse, L., and Maes, M. A., "Random Field Modeling of Elastic Properties Using Homogenization," *Journal of Engineering Mechanics*, Vol. 127, No. 1, 2001, pp. 27–36.
doi:10.1061/(ASCE)0733-9399(2001)127:1(27)
- [9] Sakata, S., Ashida, F., Kojima, T., and Zako, M., "Three-Dimensional Stochastic Analysis Using a Perturbation-Based Homogenization Method for Elastic Properties of Composite Material Considering Microscopic Uncertainty," *International Journal of Solids and Structures*, Vol. 45, Nos. 3–4, 2008, pp. 894–907.
doi:10.1016/j.ijsolstr.2007.09.008
- [10] Sakata, S., Ashida, F., and Zako, M., "Kriging-Based Approximate Stochastic Homogenization Analysis for Composite Materials," *Computer Methods in Applied Mechanics and Engineering*, Vol. 197, Nos. 21–24, 2008, pp. 1953–1964.
doi:10.1016/j.cma.2007.12.011
- [11] Clement, A., Soize, C., and Yvonnet, J., "Computational Nonlinear Stochastic Homogenization Using a Nonconcurrent Multiscale Approach for Hyperelastic Heterogeneous Microstructure Analysis," *International Journal for Numerical Methods in Engineering*, Vol. 91, No. 8, 2012, pp. 799–824.
doi:10.1002/nme.v91.8
- [12] Clement, A., Soize, C., and Yvonnet, J., "Uncertainty Quantification in Computational Stochastic Multi-Scale Analysis of Nonlinear Elastic Materials," *Computer Methods in Applied Mechanics and Engineering*, Vol. 254, Feb. 2013, pp. 61–82.
doi:10.1016/j.cma.2012.10.016
- [13] Acar, P., and Sundararaghavan, V., "Uncertainty Quantification of Microstructural Properties due to Variability in Measured Pole Figures," *Acta Materialia*, Vol. 124, 1 Feb. 2017, pp. 100–108.
- [14] Wilk, M. B., and Gnanadesikan, R., "Probability Plotting Methods for the Analysis of Data," *Biometrika*, Vol. 55, No. 1, 1968, pp. 1–17.
- [15] Ross, S. M., *Introduction to Probability Models*, 10th ed., Elsevier, New York, 2010, pp. 40, 43.
- [16] Acar, P., and Sundararaghavan, V., "Utilization of a Linear Solver for Multiscale Design and Optimization of Microstructures," *AIAA Journal*, Vol. 54, No. 5, 2016, pp. 1751–1759.
doi:10.2514/1.J054822
- [17] Simmons, G., and Wang, H., *Single Crystal Elastic Constants and Calculated Aggregate Properties*, MIT Press, Cambridge, MA, 1971, pp. 142, 143.
- [18] Sundararaghavan, V., and Zabarar, N., "A Multi-Length Scale Continuum Sensitivity Analysis for the Control of Texture-Dependent Properties in Deformation Processing," *International Journal of Plasticity*, Vol. 24, No. 9, 2008, pp. 1581–1605.
doi:10.1016/j.ijplas.2007.12.005

R. Ohayon
Associate Editor